Surface-Engineering of Ultrathin Gold Nanowires: Tailored Self-Assembly and Enhanced Stability

El Said A. Nouh, Edwin A Baquero, Lise-Marie Lacroix, Fabien Delpech, Romuald Poteau, G. Viau

Surface-engineering of ultrathin gold nanowires: tailored self-assembly and enhanced stability

El Said A. Nouh,[1] Edwin A. Baquero,[1,2] Lise-Marie Lacroix, [1] Fabien Delpech, [1] Romuald Poteau, [1] Guillaume Viau[1,*]

[1] *LPCNO, Université de Toulouse, CNRS, INSA, UPS, 135 avenue de Rangueil, F-31077 Toulouse Cedex 4, France*
[2] *Departamento de Química, Facultad de Ciencias, Universidad Nacional de Colombia, Sede Bogotá, Carrera 30 No. 45-03, 111321 Bogotá, Colombia*

* guillaume.viau@insa-toulouse.fr

Table of Content

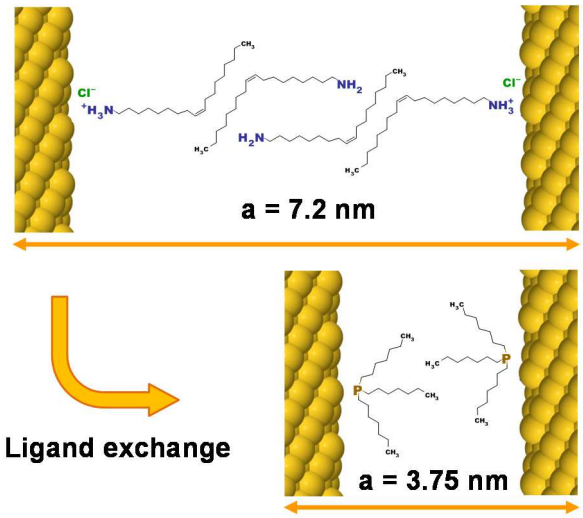

Abstract

Gold nanowires with a mean diameter of 1.7 nm were synthesized by reduction of $HAuCl_4$ in a solution of oleylamine (OY) in hexane. A bilayer of oleylammonium chloride/oleylamine at the surface of the raw nanowires was evidenced by NMR and DOSY experiments. After washing a monolayer of oleylammonium chloride remained at the surface of the nanowires. The oleylammonium chloride layer could be progressively replaced by a phosphine shell as evidenced NMR and Diffusion Ordered Spectroscopy experiment (DOSY) experiments, in good agreement with the adsorption energies given by DFT calculations. The nanowires crystallize into hexagonal superlattices with a lattice parameter that can be tailored depending on the ligand shell. Small angle X-ray scattering showed the following lattice parameters: $Au@OY^+Cl^-(OY)$ (a = 7.2 nm) > Au@TOPO/OY (a = 6.6 nm) > $Au@ OY^+Cl^-$ (a = 4.1 nm) > Au@TOP (a = 3.75 nm). This is one of few examples of surface modification of ultrathin nanowires that does not alter their morphology. Moreover, the nanowires coated with phosphines exhibited long time stability (at the opposite of other ligands like thiols) opening the way to more complex functionalization.

Introduction

Ultrathin metallic nanowires and metallic nanocontacts exhibit unique structural[1,2] and electronic[3] properties due to their very small diameter and 1D feature. Different ways of elaboration of these nanostructures were developed to measure experimentally quantum properties at room temperature.[3,4] Bottom-up synthesis routes lead to various ultrathin nanowires with applications in different fields like superconducting materials, catalysis or sensors. [4] In particular, ultrathin gold nanowires (Au NWs) are promising candidates for nanoelectronics,[5,6] as efficient electro-catalysts for the reduction of CO_2 to CO,[7] as active materials in chemical sensors,[8] or in optics with longitudinal surface plasmon resonance located in the infra-red region depending on their aspect ratio.[9] Moreover, their very high aspect ratio allows to reach a percolation threshold for very low wires volume fraction which is very interesting for transparent and conductive films.[10,11,12] Ultrathin gold nanowires prepared by wet chemistry method are also a class of flexible 1D nanostructure[13] and were used to elaborate flexible devices like pressure sensors[14] and flexible supercapacitors.[15] Directed assemblies of ultrathin gold nanowires onto surface were developed using different techniques like nano-imprinting,[12] dielectrophoresis[16] and nanoxerography[17] in order to measure wires their intrinsic properties and to master the fabrication of devices with complex architectures.

The synthesis of ultrathin Au NWs were reported in several papers.[18,19,20,21,22] In most of them gold chloride ($HAuCl_4$) is reduced either in pure oleylamine or in a solution of oleylamine in a nonpolar solvent. Theoretical study using DFT calculations suggested that the amine adsorption favored the stabilization of the {100} Au facets that could explain the anisotropic growth.[23] Nevertheless, the yield of nanowires was found much higher when oleylamine was diluted in a solvent rather than in pure oleylamine.[24] Self-assembly of ultrathin Au NWs into bundles were observed in the mother liquors and the characterization of these bundles by small angle X-ray diffraction evidenced a self-organized bi-layer of oleylamine at the surface of the wires that could also explain the anisotropic growth.[25] The structure of the oleylamine bi-layer was found very dependent on the nature of the solvent.[26]

One limitation to the use of ultrathin gold nanowires in devices is their instability.[27] Wires breakdown under the beam of the electron microscope is difficult to avoid[28] and in some cases revealed single atom chain as transient state.[29] Aging in solution leads also to a fragmentation due to Rayleigh instability[30] explaining that the electronic

properties measured on assemblies of wires are that of shorter fragments.[31] Only very few studies dealt with the stability improvement of the ultrathin gold nanowires prepared by wet chemistry. A silica coating of Au ultrathin wires was developed that improved their thermal stability but also their ageing in solutions at different pH.[32] It was also described that oleylamine concentration plays an essential role in the stability of ultrathin gold nanorods.[30] It is very likely that the nanowire surface chemistry may have a strong impact on their stability and that ligand exchange may modify this stability. While the ligand exchange at the surface of ultra-small gold nanoparticles has been deeply studied with a lot of applications such as functionalization for biology, self-assembly or catalytic properties,[33] there is almost no such studies in case of ultrathin Au NWs. Only one paper showed that the replacement of oleylamine by a long-chain amidoamine derivative as ligand in the synthesis makes the ultrathin gold nanowires water-dispersible.[34]

In this paper we report on the ligand exchange at the surface of ultrathin Au NWs and on the characterization of this exchange by NMR and small angle X-ray diffraction. We show that a ligand exchange has strong consequences on the Au NWs self-assembly and on their stability in solution.

Experimental

Materials

Hydrogen tetrachloroaurate tri-hydrate ($HAuCl_4$, $3H_2O$) was purchased from Alfa Aesar, oleylamine 80-90% (OY) from Across Organic. Triisopropylsilane (TIPS), trioctylphosphine (TOP), trioctylphosphineoxide (TOPO), hexane and absolute ethanol were obtained from Sigma-Aldrich.

Ultrathin gold nanowires synthesis

Ultrathin gold nanowires (Au NWs) were synthesized according to a protocol adapted from Feng *et al.*[21]. In a typical synthesis, 20 mg of $HAuCl_4 \cdot 3H_2O$ (10 mM) was dissolved in a solution containing, 0.68 mL of oleylamine (400 mM) and 3.3 ml of hexane. Then, 1.02 ml (1M) of triisopropylsilane (TIPS) was added to the solution to initiate the reduction process. The solution was kept at 25°C for 24 h without stirring.

Purification protocol

The gold nanowire suspensions were subjected to purification and ligand exchange. One cycle of purification (1-purif) consisted in the following sequence: 5 mL of absolute ethanol were added to 2.5 mL of the as prepared Au NWs suspension, the mixture was centrifuged at 4000 rpm for 5 min and the supernatant was discarded. The precipitate was redispered in 2.5 mL of hexane for stability assessment and in 1 mL for SAXS measurements. Two purifications (2-purif) consisted to repeat this cycle once again on the washed suspension.

Ligand exchange

Oleylamine was exchanged by trioctylphosphine (TOP) and trioctylphosphine oxide (TOPO) according to the following protocol. First, 500 µL of the suspension of Au NWS in hexane were washed with ethanol (1mL), centrifuged at 4000 rpm for 5 min and redispersed in 500 µL of hexane. Then, 500 µL of a solution of 10 mM of TOP (or TOPO) were added to the purified Au NWs in hexane. These suspensions were characterized after aging for different times at 25°C. The suspensions were characterized as such and purified following the same procedure as described above. The TOP solutions were handled in a glove box to avoid the TOP oxidation.

Characterizations

The transmission electron microscopy (TEM) characterizations were performed using a JEOL 1011 microscope operating at 100 kV. A drop of gold nanowire suspension in hexane was deposited on a carbon-coated copper grid and dried under vacuum.

Small Angle X-ray Diffraction was performed on a PANalytical Empyrean diffractometer equipped with a Cobalt source, λ (Co Kα1/Kα2) = 1.7889/1.792Å, a Bragg-Brentano HD optics with a divergence slit of 1/32° and an anti-scatter slit of 1/8°, and a PIXcel1D-Medpix3 detector. Several drops of gold nanowire suspension in hexane were deposited on a zero-background silicon substrate and then dried at room temperature for 3 min.

Solution NMR spectra were obtained on a Bruker Avance I 500 spectrometer equipped with a 5 mm triple resonance inverse Z-gradient probe (TBI ^{1}H, ^{31}P, BB). ^{1}H NMR spectrum were recorded in toluene-d_8 at 293 K. Diffusion measurements were made using the stimulated echo pulse sequence. The mixing time of NOESY experiment were set to 100 ms. Chemical shifts (δ, parts per million) are quoted relative to $SiMe_4$ (^{1}H). They were measured by internal referencing to the residual ^{1}H resonances of the deuterated solvent (toluene-d_8, ^{1}H δ 2.09 as a quintuplet of the methyl group). ^{31}P chemical shifts were referenced to an external 85% H_3PO_4 sample.

Density Functional Theory calculations

As already done in our previous paper,[24] the electronic properties of [111] oriented bulk AuNWs were calculated within the framework of the DFT considering periodic boundary conditions and the spin polarized constraint. These [111] direction oriented AuNWs, were generated by cleaving fcc bulk Au with low index surfaces. The exchange-correlation potential was approximated by the generalized gradient approach proposed by Perdew, Burke, and Ernzerhof (PBE).[35] Calculation of the energetic parameters as well as the geometry optimizations were carried out using the projector augmented waves (PAW) full-potential reconstruction[36,37] implemented in the Vienna ab initio simulation package, VASP.[38,39] To minimize errors arising from the frozen core approximation, we used the PAW data sets treating the 4p, 4d and 5s Au states (17 valence electrons). A kinetic energy cutoff of 525 eV was sufficient to achieve a total energy convergence within several millielectronvolts for ligands adsorption. van der Waals interactions were taken into consideration by adding a pairwise interatomic term E_{disp} to the Kohn−Shan DFT energies, which was evaluated

using the revised DFT-D3 method of Grimme with Becke-Jonson damping.[40],[41] For the geometry optimizations, a (1×1×11) Γ-centered [42] *k*-points grid was used to sample the reciprocal space combined with a Gaussian smearing of 0.02 eV width for the partial occupancies. Atoms were free to move until the residual forces on any direction were less than 0.02 eV/Å. The supercell size along the *a* and *b* directions is set to ensure a vacuum space of *ca.* 14 Å between periodic images of decorated Au NWs.

Results and Discussion

1. Au NWs characterizations

Figure 1 shows a TEM image of Au NWs prepared by the reduction of $HAuCl_4 \cdot 3H_2O$ dissolved in a solution of oleylamine in hexane with TIPS at 25°C. The wire mean diameter is d = 1.7 nm and the standard deviation of the diameter distribution is very small as already observed by several studies. [21,25] Several drops of a suspension in hexane of Au NWs purified one time were evaporated on the XRD zero background silicon substrate. The X-ray diffraction pattern of the dry assembly exhibited several peaks at small angles revealing the crystallization of the NWs in a hexagonal phase. The peak positions in the reciprocal space relative to the position of the first peak were 1:√3:√4:√7:√9:√12:√13 (Fig. 2a) characterizing a bidimensional hexagonal positional order in the plane normal to the wires. The lattice parameter *a* calculated as the average of the distance of the different *(hk)* reflections $d_{(hk)} = \frac{a}{\sqrt{h^2+k^2+hk}}$ was found equal to 7.2 nm. In such hexagonal array the parameter *a* corresponds to the inter-wire distance. [25] The spacing between the wires is thus estimated to $e = a - d = 5.5$ nm (with *d* the wire diameter of 1.7 nm). Additional peaks corresponding to the (00*l*) reflections of pure oleylamine were also observed (Fig. 2a) showing an excess of OY that crystallized on the substrate at room temperature.

The XRD pattern at small angles of the same nanowires purified twice revealed also the formation of a hexagonal phase but with (*hk*) reflections strongly shifted to high q (Fig. 2b). This shift reveals a much smaller lattice parameter $a = 4.1$ nm and a corresponding spacing between the wires $e = a - d = 2.4$ nm. The peaks of pure oleylamine did not appear on the XRD pattern in agreement with an efficient washing that removed the free oleylamine molecules from the suspensions purified twice (Fig. 2b).

Previous studies described the self-assembly of ultrathin Au NWs into hexagonal phase in solution. In situ small angle X-ray scattering experiments carried out on as-synthesized suspensions showed the formation after a few hours of a hexagonal phase with a lattice parameter $a = 9.7$ nm.[25] This very large parameter compared to the oleylamine length in all-trans configuration (2.1 nm) was explained by a bi-layer of oleylamine around the Au NWs. Recently, Reiser *et al.* showed that the lattice

parameter of the Au NWs hexagonal phase that crystallized in the mother liquor strongly depends on the oleylamine volume fraction in the solution. They found a variation between 10.2 nm and 7.5 nm when the OY volume fraction was varied between 0.05 and 0.75, respectively. [26] This variation was interpreted as the result of a progressive interdigitation of the OY molecules surrounding the wires due to an increasing osmotic pressure when the concentration of free OY was increased.[26] The lattice parameter of 7.2 nm measured on the dried nanowires is in good agreement with this variation. In the present case hexane was evaporated that could provoked an even stronger interdigitating. Nevertheless, the large interwire spacing (5.5 nm) compared to the length of a single OY molecules supports that the Au NWs after one purification are still coated by a bilayer of oleylamine molecules with a strong interdigitation.

After two purifications the shortening of the distance between the wires in the hexagonal phase can be explained by the removal of the external layer of OY leading to a single OY layer at the surface of the wires. Considering that OY has a length of 2.1 nm in all-trans configuration, the spacing of 2.4 nm means that the OY molecules strongly interdigitate. A scheme of the interwire spacing in the different distance hexagonal phases is proposed on figure 10.

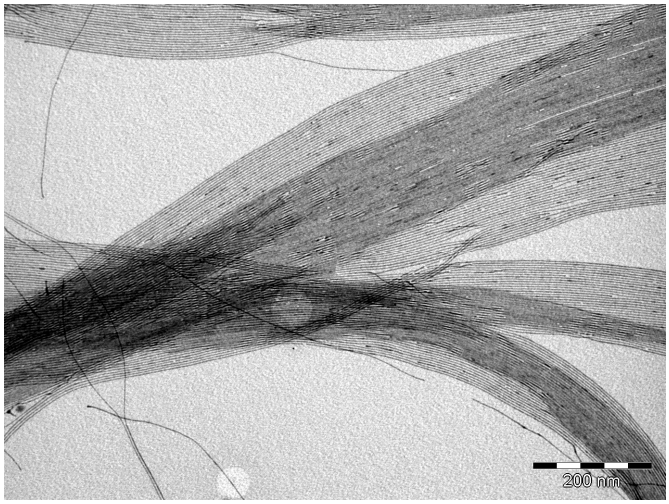

Figure 1. TEM image of Au NWs synthesized by reduction with TIPS of a solution of $HAuCl_4 \cdot 3H_2O$ in a solution hexane containing oleylamine at 25°C for 24 h.

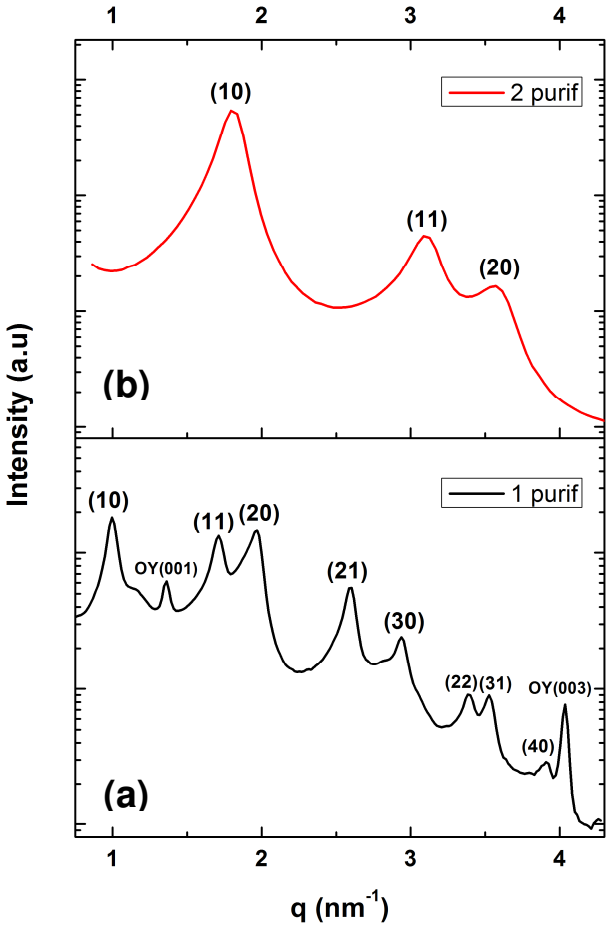

Figure 2. X-ray diffraction pattern at small angles of Au NWs deposited and dried on a zero-background silicon substrate (a) wires purified one time and (b) wires purified twice.

Suspensions of Au NWs after one and two purifications were characterized by solution ^{1}H NMR spectroscopy in toluene-d_8. In the spectrum of the sample purified one time resonance signals were found at 5.51, 2.55, 1.45, 1.35–1.15, and 0.95 ppm that are attributed to the alkene, the CH_2 alpha to the NH_2, the CH_2 beta to the NH_2, the 13 CH_2 and the methyl groups of oleylamine, respectively (Fig. 3a). The Diffusion Ordered Spectroscopy experiment (DOSY) gave a diffusion coefficient of 1.0 10^{-9} $m^2.s^{-1}$. This value is similar to that found for pure OY (1.1 x 10^{-9} $m^2.s^{-1}$, Fig. S1) and it is thus attributed to free OY due to the large excess present in the suspension in agreement with the results found by SAXS.

In the ^{1}H NMR spectrum of the Au NWs purified twice the resonance signal attributed to the CH_2 alpha and beta to the NH_2 group were shifted to 2.82 and to 1.79 ppm, respectively (Fig. 3b). This downfield shift compared to the resonance signals of the free OY is attributed to the presence of oleylammonium chloride in the sample that was not detectable in the sample purified only one time. The presence of oleylammonium was confirmed by the resonance signal centered at 8.85 ppm assigned to the $-NH_3^+$ cation (Fig. 3b). Moreover, the resonances of the CH_2 alpha and beta to the NH_3^+ group are broadened revealing the coordination of the oleylammonium to the Au NWs surface. Indeed, the reduced mobility of the ligands bound to a nanoparticle induces the NMR lines broadening and this effect is more marked for the protons closest to the surface.[43,44,45,46] Additionally, a confirmation of the coordination of oleylammonium to Au NWs is given by the diffusion coefficient measurements obtained from DOSY experiments (Fig. S2). Whereas the diffusion coefficient found for free OY in this sample was $8.9\ 10^{-10}\ m^2.s^{-1}$, the oleylammonium displayed a significant lower value ($4.0\ 10^{-10}\ m^2.s^{-1}$).

The presence of oleylammonium is probably due to the presence of an acid proton in the gold precursor $HAuCl_4$, 3 H_2O. Previous theoretical calculations suggested that that the adsorption of ammonium chloride was more favorable than amine at the surface of gold nanowires.[24] The modification of the ligand shell with washing suggests a first coordination shell containing mainly the ammonium and a second shell containing mainly the amine. In the sample washed only one time the excess of free amine hides the signal of the ammonium shell.

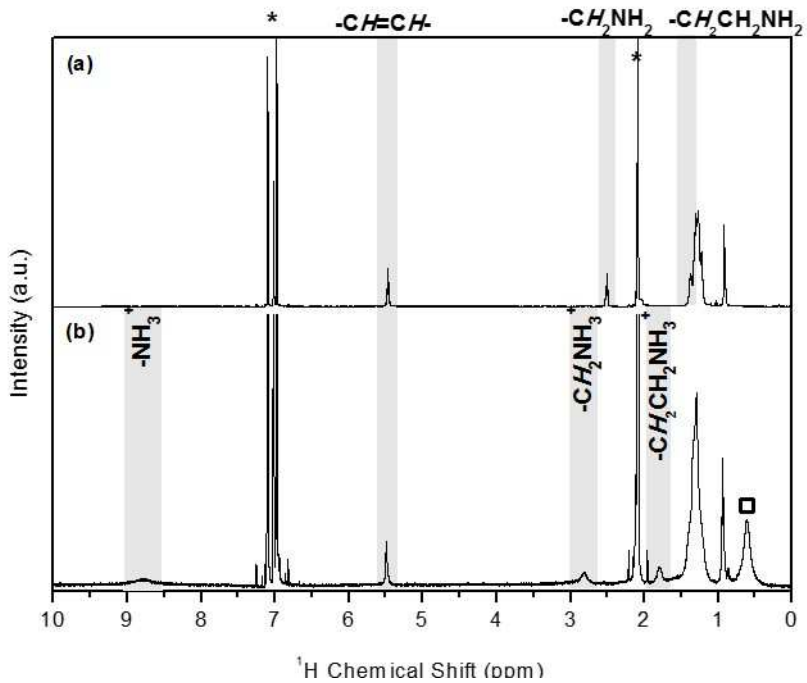

Figure 3. ^{1}H NMR spectra of Au NWs coated by oleylamine/oleylammonium shells after (a) one purification and (b) two purifications (*:toluene-d_8, □: water).

2. Ligand exchange

A solution of trioctylphosphine (TOP) in hexane (10 mM) was added to a dispersion in hexane of nanowires purified one time (gold concentration = 10 mM). X-ray diffraction patterns at small angle were recorded at different times after the addition of TOP. Several drops of the suspension were deposited and dried on the zero-background Si substrate. On figure 4 are given the XRD patterns recorded after a contact time between the wires and TOP of 30 min and 72h. In both cases the wires crystallize in a single hexagonal phase with a lattice parameter significantly lower than the lattice parameter of 7.2 nm measured on the purified nanowires coated by oleylamine. The observation of a single phase, and not a mixture of two phases, is consistent with a progressive ligand exchange in the NW coordination shell, the lattice parameter being a mean value of the interwire distances. After only 30 min of contact time the lattice parameter was found a = 4.85 nm (Fig. 4a) and after 72h it decreased to reach a = 3.75 nm (Fig. 4b).

The same experiments were done with trioctylphosphine oxide TOPO (Fig. 5). The wires crystallized in a hexagonal phase with a lattice parameter significantly higher than with TOP, a = 6.6 nm, and that did not vary when the time was increased from 30 min to 72 h.

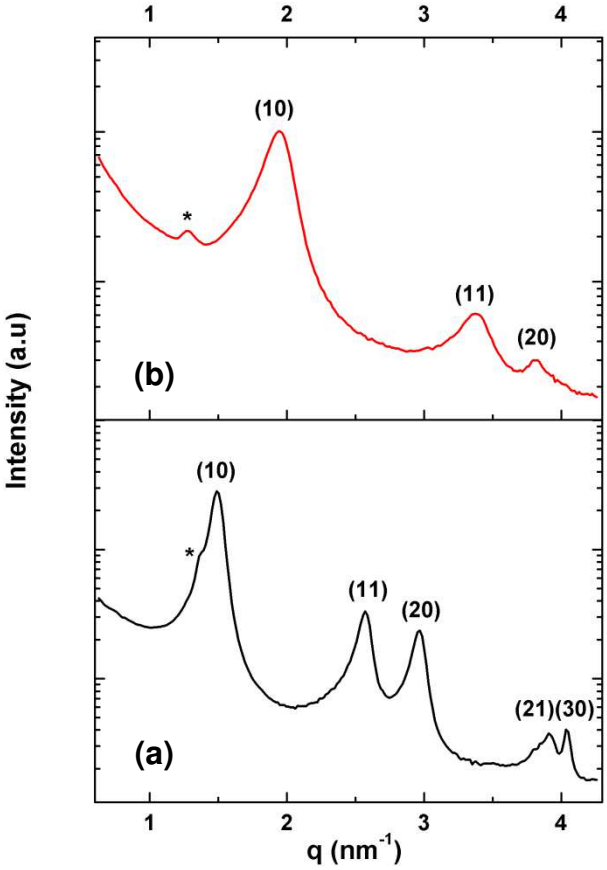

Figure 4. X-ray diffraction patterns at small angle of Au NWs aged in a solution of TOP for different times: (a) 30 min ; (b) 72 h. (*OY peaks are marked with a star).

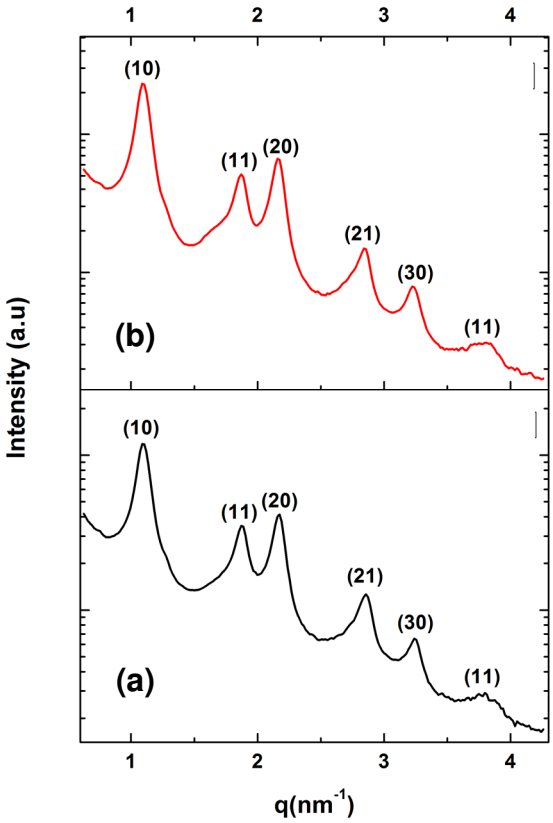

Figure 5. X-ray diffraction patterns at small angle of Au NWs aged in a solution of TOPO for different times: (a) 30 min ; (b) 72 h.

In order to follow the coordination of TOP and TOPO ligands at the surface of the Au NWs, solution NMR analysis were performed after ligand exchange and after different cycles of purification.

After the addition of TOP, a resonance signal centered at - 32.3 ppm was detected in the ^{31}P NMR spectrum. This peak was assigned to free TOP. After one and two purifications, this resonance was not detected anymore by solution ^{31}P NMR spectroscopy (Figure S3) meaning that free TOP was no more present in the sample. The same result was found when the ligand exchange was made with TOPO. After either one or two purifications, no free TOPO (δ 42.4 ppm) was detected by ^{31}P NMR (Figure S4). In the ^{1}H NMR spectra of the samples treated with TOP after both, one and two purifications, the resonance signal centered at 1.6 ppm is attributed to the CH_2 group in alpha to the phosphorous atom indicating the presence of TOP at the

surface of the wires. The resonance signal is broadened and slightly shifted to higher frequencies compared to the same resonance signal in the free TOP (1.5 ppm) due to the coordination of TOP to the wires (Figure 6b, c and d). Interestingly, the signal of oleylammonium is no more present suggesting the full replacement of this ligand by the phosphine. Additionally, the peaks at 5.51 and 2.55 ppm assigned to the alkene and the CH_2 alpha to the NH_2 of OY are also detected and this confirms the residual presence of OY as observed by SAXS. Consistently, the DOSY experiments evidenced two diffusion coefficients in the sample purified twice, 1.4 x 10^{-9} $m^2.s^{-1}$ and 2.2 x 10^{-10} $m^2.s^{-1}$. The first coefficient is assigned to free OY while the second is assigned to coordinated TOP since the diffusion filtered spectrum at 2.2 x 10^{-10} $m^2.s^{-1}$ only shows the resonances of TOP (Fig. S5). These results together with those obtained by ^{31}P NMR suggest that TOP has replaced oleylammonium and is tightly bound to the surface of Au NWs. This is confirmed by periodic-DFT calculations, aiming at evaluating the adsorption energy of surface species on a 1.7 nm Au NW. The results are summarized in Figures 10 and S6. As already explained in Ref. 24, the methylammonium chloride ion pair, with the polar ammonium head lying above an adsorbed chloride, binds weakly at the Au NW surface (-19.1 $kcal.mol^{-1}$), whereas its adsorption is significantly enhanced if both moieties are simultaneously adsorbed. Such adsorption can result in an alternant positive/negative pattern that enhances adsorption strength (-40.1 $kcal.mol^{-1}$ per ion pair). Regarding the adsorption of TOP, we considered a smaller molecular model, PMe_3, in order to reduce the computational effort. Such model provides a lower limit of the adsorption strength of σ-donor phosphines. It turns out that the σ-donor character of the trimethylphosphine ligand is already strong, with an adsorption energy of -43.4 $kcal.mol^{-1}$, 20 $kcal.mol^{-1}$ stronger than the adsorption of the trimethylamine counterpart (a detailed comparison of the electronic structure of grafted amines and phosphines is given in the supporting information document. In short, a smaller HOMO-LUMO gap in PMe_3 and a significant ligand-to-metal charge transfer interaction observed when grafted to the metal surface, account for a stronger adsorption energy). This result suggests that the surface adsorption of TOP on AuNW surface is a thermodynamic driving force that breaks the ionic interactions and that explains the exchange between ammonium and TOP ligands.

The progressive decreased of the interwire distance is explained by a progressive substitution of the OY by TOP that exhibit shorter chains. Au NWs aged 72 h with TOP crystallized in a hexagonal phase with a very short lattice parameter of 3.75 nm corresponding to an interwire spacing of only 2 nm, i.e. lower than the oleylamine length. This value suggests a nearly complete exchange of OY by TOP (Fig. 10).

Regarding to the Au NWs treated with TOPO, in the ^{1}H NMR spectra of the samples after one and two purifications, the resonances of oleylammonium are again lacking while those of OY and TOPO can be observed. The signal at $\delta = 1.6$ ppm attributed to the CH_2 group in alpha to the phosphorous atom was broadened compared to free TOPO (Fig. 7b, c and d), suggesting that TOPO is coordinated to the surface. The presence of TOPO molecules in the first coordination shell was confirmed by DOSY experiments. Two diffusion coefficients were found, 9.1 10^{-10} $m^2.s^{-1}$ and 1.29 10^{-10} $m^2.s^{-1}$, attributed respectively to OY and TOPO thanks to the diffusion filtered spectrum (Fig. S7). However, in contrast to the sample treated with TOP, the signals of the alkene and CH_2 alpha to NH_2 of OY are slightly more intense in the sample treated with TOPO (Fig. 7a,d) suggesting a less efficient exchange with TOPO than with TOP. A larger amount of oleylamine remaining in the coordination shell of the NWs could explain a larger interwire distance. With TOPO the lattice parameter of the NW array after 72 h takes an intermediate value between the parameter measured on the nanowires coated by oleylammonium chloride oleylamine and those after TOP exchange. This suggests that the oleylamine exchange is incomplete with TOPO while almost complete with TOP. This finding can be rationalized in terms of hard–soft acid–base (HSAB) principle.[47] Au nano-objects with soft surface sites form stronger bond with the soft P atom (i.e. TOP) than with the hard O atom (i.e. TOPO).

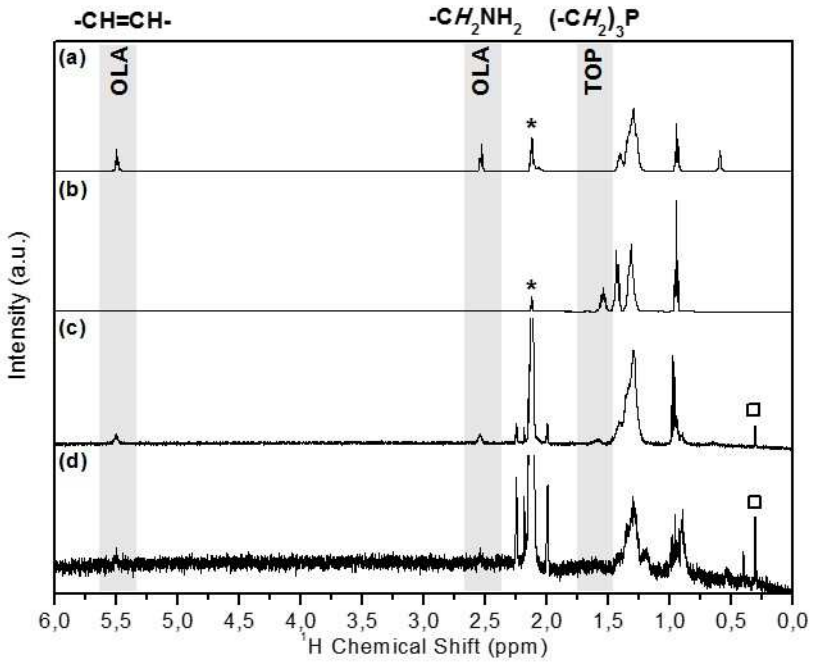

Figure 6. ^{1}H NMR spectra of (a) oleylamine, (b) trioctylphosphine, (c) Au NWs coated by oleylamine exchanged with TOP after one purification, and (d) after two purifications (*:toluene-d_8, □: water).

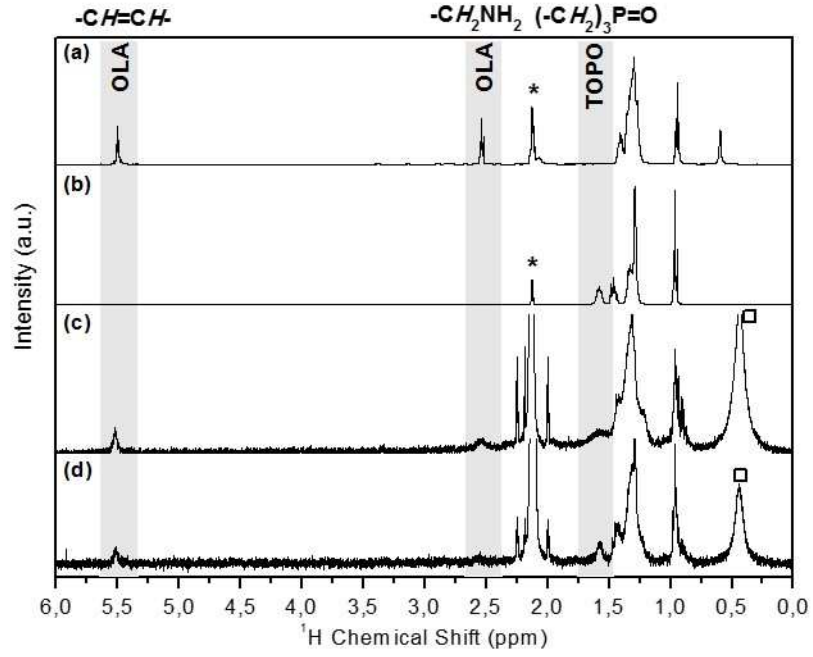

Figure 7. ^{1}H NMR spectra of (a) oleylamine, (b) trioctylphosphine oxide, (c) Au NWs coated by oleylamine exchanged with TOPO after one purification, and (d) after two purifications (*:toluene-d_8, □: water).

3. Au NWs stability

The stability of the nanowires in solution was followed by examining the evolution of morphology by TEM and superlattices formation by XRD during 13 days. On Figure 8 are presented the SAXS pattern and the corresponding TEM images of Au NWs purified one time and aged in solution for different time intervals. After 7 days one can notice that the peak intensity of the NW hexagonal array decreased and the super-lattice disappeared completely after 13 days, peaks corresponding to pure oleylamine only remain (Fig. 8c). The full width at half height, Δq, of the (10) peak reported in table 1 showed a progressive broadening with time meaning that the coherence length of the hexagonal array, estimated to $L_{coh} = 2\pi/\Delta q$, decreased continuously. The TEM images showed that the mean diameter of the Au wires increased after 7 days that explained the loss of coherence of the hexagonal lattice. After 13 days the ultrathin NWs totally disappeared. Anisotropic particles were still observed but their mean diameter increased to a mean value of 11 nm with a large size distribution and no long range order was visible in agreement with the SAXS pattern.

Figure 9 shows the effect of aging on SAXS measurements and the corresponding TEM images of Au NWs stabilized by TOP and TOPO. Even after 13 days of aging in solution the Au NWs kept their morphology and the hexagonal arrays were still observed by SAXS. The peak broadening observed for short contact time with TOP and TOPO compared to the original hexagonal array (Tab. 1) is likely due to parameter fluctuations due to the progressive shell replacement of oleylammonium chloride by the phosphines. After 3 days of contact time this peak broadening is stabilized showing the absence of any further evolution.

Phosphines are good ligands to preserve the NW morphology and to improve their stability with time in solution. At the opposite when we tried to make ligand exchange with 1-dodecanthiol, we found that this ligand destroys the Au NWs even at low concentrations (Fig. S8).

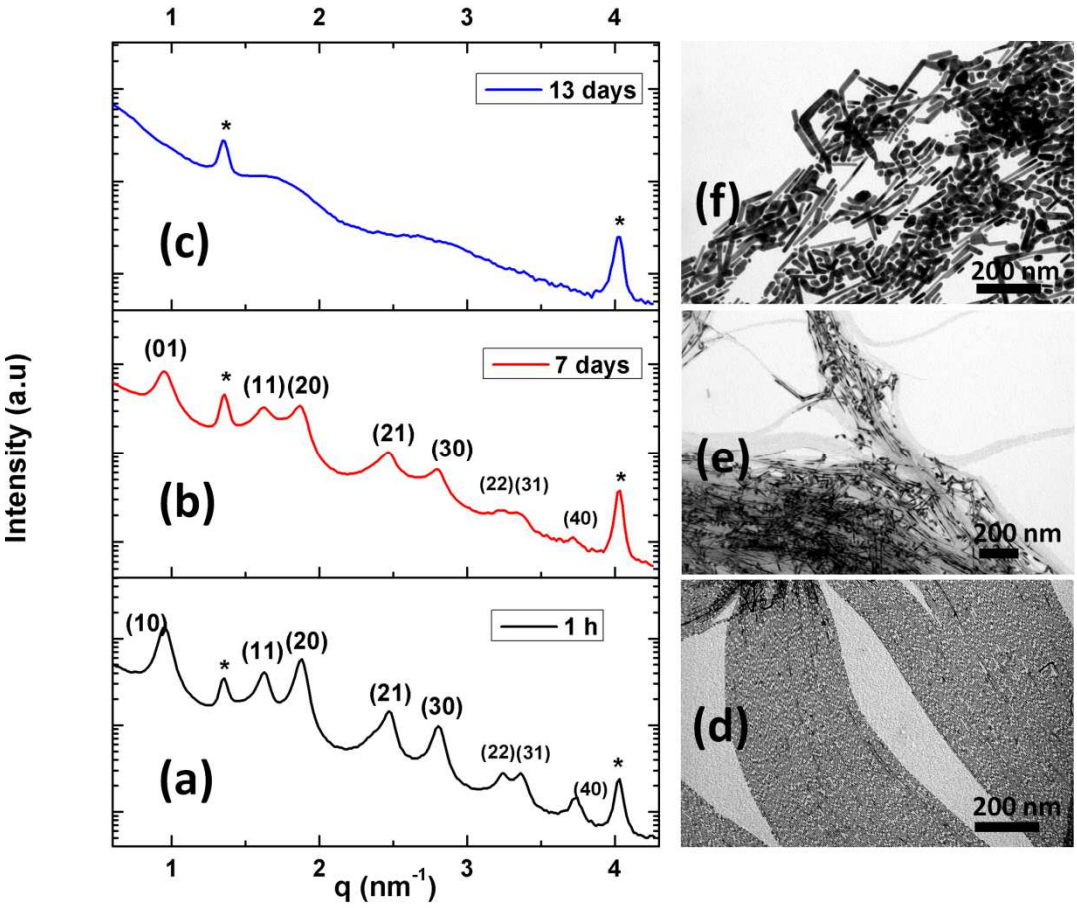

Figure 8. Effect of time on Au NWs prepared at 25 °C: SAXS patterns after 0, 7 and 13 days (a, b, c) and corresponding TEM images (d, e, f).

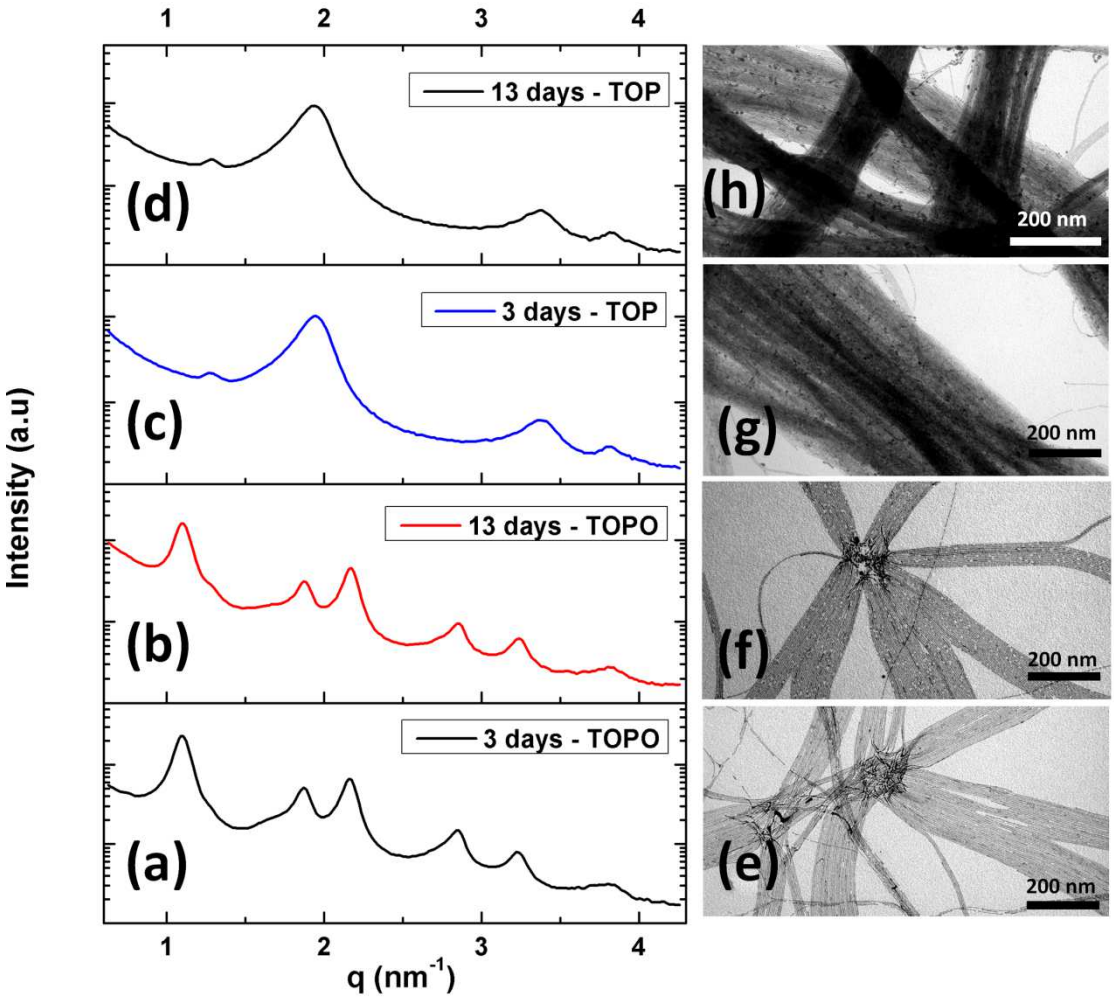

Figure 9. Effect of time on Au NWs after TOPO and TOP ligand exchange: SAXS measurements after 3 and 13 days (a, b)with TOPO, and (c, d) with TOP; corresponding TEM images after 3, 13 days (e, f) TOPO and (g, h) TOP.

Table 1. Effect of time on Au NWs stabilized by oleylamine and after TOP and TOPO ligand exchange on the FWHM (Δq) of the (10) peak. For the pure oleylamine shell the corresponding coherence length L=2π/Δq is given.

Time (day)	OY		TOP	TOPO
	Δq (nm^{-1})	L (nm)	Δq (nm^{-1})	Δq (nm^{-1})
0	0.085	75	0.13	0.14
3	0.24	26	0.25	0.13
9	0.34	18	0.26	0.13
13	-	-	0.26	0.13

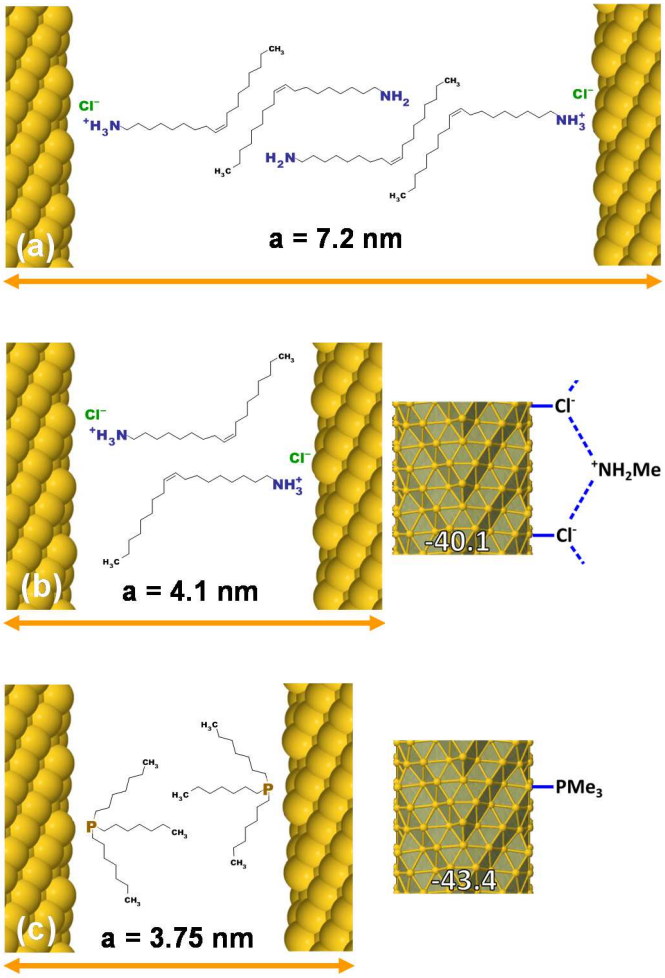

Figure 10. Schematic representations of the ligand shell of Au NWs and interwire distance: (a) after 1 purification ; (b) after 2 purifications and (c) after exchange with TOP. Right: adsorption energies of methyl ammonium chloride and trimethylphosphine calculated by periodic-DFT.

Summary and conclusion

Gold ultrathin nanowires (Au NWs) with a mean diameter of 1.7 nm were synthesized by reduction of $HAuCl_4$ in a solution of oleylamine in hexane. The oleylamine (OY) was then exchanged by trioctylphosphine (TOP) and trioctylphosphine oxide (TOPO). SAXS and NMR characterizations were carried out on the Au NWs in dried state and in solution, before and after ligand exchange.

Hexagonal arrays of parallel nanowires were evidenced by SAXS. This technique presents the advantage over transmission electron microscopy to characterize large amount of samples and not only local area. The formation of hexagonal arrays of nanowires requires monodisperse wires and well-defined ligand shell. The lattice parameter of the hexagonal arrays gives the mean interwire distance and the spacing between the wires is calculated by subtracting their mean diameter. We observed that the lattice parameter decreased when oleylamine was removed by washing and the interwire distances are consistent with wires coated by a bilayer of oleylamine that becomes a monolayer after washing. ^{1}H NMR allowed to precise that the first coordination shell consisted mainly in oleylammonium suggesting the presence of chloride ions bound to the gold surface in agreement with adsorption energy calculations by periodic DFT.

The oleylamine/oleylammonium bilayer was modified by ageing nanowires suspensions in TOP and TOPO solutions in hexane. NMR showed that the oleylammonium chloride shell was completely removed by TOP and TOPO. This experimental result was confirmed by DFT calculation showing a stronger adsorption of phosphines on the Au NWs. NMR showed also that OY molecules remained with TOPO while they were almost completely replaced by TOP. The ligand shell modification changed the lattice parameter of the NWs hexagonal arrays. The following order of the lattice parameters was found: Au@$Cl^{-}OY^{+}$ (OY) (a = 7.2 nm) > Au@TOPO/OY (a = 6.6 nm) > Au@$Cl^{-}OY^{+}$ (a = 4.1 nm) > Au@TOP (a = 3.75 nm). The two first values are explained by a bilayer of ligand at the surface of the Au NWs while the two last values are explained by a monolayer (Fig. 10) in agreement with the DOSY experiments.

In conclusion we have showed that it is possible to tailor the interwire distance of ultrathin gold nanowires in hexagonal array playing on the ligand shell. This study showed also that Au NWs coordinated by TOP and TOPO exhibit long time stability in solution which is an important prerequisite for further applications and it opens the way to more complex functionalization.

Acknowledgement

E. S. A. Nouh thanks the French Institute in Cairo (Egypt), the Science and Technology Fund (STDF) and Institut National des Sciences Appliquées of Toulouse for awarding a Fellowship to support this research. E. S. A. Nouh gratefully acknowledges the help from Egyptian Nuclear Materials Authority (Cairo) for granting him a sabbatical leave to carry out this work at LPCNO. E.A.B. is grateful to Marie Curie Actions and Campus France for a PRESTIGE post-doc fellowship (FP7/2007-2013) under REA grant agreement n° PCOFUND-GA-2013-609102. This work was supported by Programme Investissements d'Avenir under the program ANR-11-IDEX-0002-02, reference ANR-10-LABX-0037-NEXT. We thank Yannick Coppel and Christian Bijani for NMR measurements. R. Poteau also acknowledges the CALcul en MIdi-Pyrénées HPC (CALMIP-EOS, grant P0611) for its generous allocation of computational resources.

References

(1) Gülseren, O.; Ercolessi, F.; Tosatti, E. Noncrystalline Structures of Ultrathin Unsupported Nanowires, *Phys. Rev. Lett.* **1998***, 80*, 3775-3778.

(2) Kondo, Y.; Takayanagi, K. Synthesis and Characterization of Helical Multi-Shell Gold Nanowires, *Science* **2000**, *289*, 606-608.

(3) Requist, R.; Baruselli, P. P.; Smogunov, A.; Fabrizio, M.; Modesti, S.; Tosatti, E. Metallic, Magnetic and Molecular Nanocontacts. *Nature Nanotech.* **2016**, *11*, 499–508.

(4) Liu, H.; Li, L.; Scofield, M. E.; Wong, S. S. Research Update: Synthesis, properties, and applications of ultrathin metallic nanowires and associated heterostructures, *APL Mater.* **2015**, *3*, 080701.

(5) Chandni, U.; Kundu, P.; Kundu, S.; Ravishankar, N.; Ghosh, A. Tunability of Electronic States in Ultrathin Gold Nanowires *Adv. Mater.* **2013**, *25*, 2486–2491.

(6) Pud, S.; Kisner, A.; Heggen, M.; Belaineh, D.; Temirov, R.; Simon, U.; Offenhäusser, A.; Mourzina, Y.; Vitusevich, S. Features of Transport in Ultrathin Gold Nanowire Structures. *Small* **2013**, *9*, 846-852.

(7) Zhu, W.; Zhang, Y. J.; Zhang, H.; Lv, H.; Li, Q.; Michalsky, R.; Peterson, A. A.; Sun, S. Active and Selective Conversion of CO_2 to CO on Ultrathin Au Nanowires, *J. Am. Chem. Soc.* **2014**, *136*, 16132−16135.

(8) Muratova, I. S.; Mikhelsona, K. N.; Ermolenkoa, Y. E.; Offenhäusserb, A.; Mourzina, Y. Chemiresistors Based on Ultrathin Gold Nanowires for Sensing Halides, Pyridine and Dopamine, *Sensors and Actuators B* **2016**, *232*, 420–427.

(9) Takahata, R.; Yamazoe, S.; Koyasu, K.; Tsukuda, T. Surface Plasmon Resonance in Gold Ultrathin Nanorods and Nanowires, *J. Am. Chem. Soc.* **2014**, *136*, 8489−8491.

(10) Sánchez-Iglesias, A. ; Rivas-Murias, B. ; Grzelczak, M.; Pérez-Juste, J. ; Liz-Marzán, L. M. ; Rivadulla, F. ; Correa-Duarte, M. A. Highly Transparent and Conductive Films of Densely Aligned Ultrathin Au Nanowire Monolayers, *Nano Lett.* **2012**, *12*, 6066−6070.

(11) Chen, Y.; Ouyang, Z.; Gu, M;. Cheng, W. Giant Metal Superlattice Nanomembranes From Ultrathin Gold Nanowires, *Adv. Mater.* **2013**, *25*, 80-85.

(12) Maurer, J. H. M.; González-García, L.; Reiser, B.; Kanelidis, I.; Kraus, T. Templated Self-Assembly of Ultrathin Gold Nanowires by Nanoimprinting for Transparent Flexible Electronics. *Nano Lett.* **2016**, *16*, 2921−2925.

(13) Yuan, B.; Cademartiri, L. Flexible One-Dimensional Nanostructures: A Review. *J. Mater. Sci. Technol.* **2015**, *31*, 607–615.

(14) Gong, S.; Schwalb, W.; Wang, Y.; Chen, Y.; Tang, Y.; Si, J.; Shirinzadeh, B.; Cheng, W. A Wearable and Highly Sensitive Pressure Sensor with Ultrathin Gold Nanowires, *Nat. Commun.* **2014**, *5*, 3132.

(15) Gong, S. Y. Zhao, Q. Shi, Y. Wang, L. Wei Yap and W. Cheng, Self-assembled Ultrathin Gold Nanowires as Highly Transparent, Conductive and Stretchable Supercapacitor, *Electroanalysis* **2016**, *28*, 1–8.

(16) Venkatesh, R.; Kundu, S.; Pradhan, A.; Phanindra Sai, T.; Ghosh, A.; Ravishankar, N. Directed Assembly of Ultrathin Gold Nanowires over Large Area by Dielectrophoresis, *Langmuir* **2015**, *31*, 9246−9252.

(17) Moutet, P.; Lacroix, L.-M.; Robert, A.; Impéror-Clerc, M.; Viau, G.; Ressier, L. Directed Assembly of Single Colloidal Gold Nanowires by AFM Nanoxerography. *Langmuir* **2015**, *31*, 4106–4112.

(18) Halder, A.; Ravishankar, N. Ultrafine Single-Crystalline Gold Nanowire Arrays by Oriented Attachment. *Adv. Mater.* **2007**, *19*, 1854−1858.

(19) Lu, X.; Yavuz, M. S.; Tuan, H.-Y.; Korgel, B. A.; Xia, Y. Ultrathin Gold Nanowires Can Be Obtained by Reducing Polymeric Strands of Oleylamine−AuCl Complexes Formed via Aurophilic Interaction. *J. Am. Chem. Soc.* **2008**, *130*, 8900−8901.

(20) Huo, Z.; Tsung, C.; Huang, W.; Zhang, X.; Yang, P. Sub-Two Nanometer Single Crystal Au Nanowires. *Nano Lett.* **2008**, *8*, 2041−2044.

(21) Feng, H.; Yang, Y.; You, Y.; Li, G.; Guo, J.; Yu, T.; Shen, Z.; Wu, T.; Xing, B. Simple and Rapid Synthesis of Ultrathin Gold Nanowires, their Self-assembly and Application in Surface-enhanced Raman Scattering. *Chem. Commun.* **2009**, 1984.

(22) Kang, Y.; Ye, X.; Murray, C. B. Size- and Shape-Selective Synthesis of Metal Nanocrystals and Nanowires Using CO as a Reducing Agent. *Angew. Chem., Int. Ed.* **2010**, *49*, 6156−6159.

(23) You, H.; Liu, X.; Liu, H.; Fang, J. Theoretical Description of the Role of Amine Ssurfactant on the Anisotropic Growth of Gold Nanocrystals. *Cryst. Eng. Comm.* **2016**, *18*, 3934–3941.

(24) Loubat, A.; Lacroix, L.-M.; Robert, A.; Impéror-Clerc, M.; Poteau, R.; Maron, L.; Arenal, R.; Pansu, B.; Viau, G. Ultrathin Au Nanowires: Soft-Templating vs Liquid Phase Synthesis, a Quantitative Study *J. Phys. Chem.* C **2015***, 119*, 4422-4430.

(25) Loubat, A.; Imperor-Clerc, M.; Pansu, B.; Meneau, F.; Raquet, B.; Viau, G.; Lacroix, L.-M. Growth and Self Assembly of Ultrathin Au Nanowires into Expanded Hexagonal Superlattice Studied by in situ SAXS *Langmuir* **2014**, *30***,** 4005–4012.

(26) Reiser, B.; Gerstner, D. J.; Gonzalez-Garcia, L.; Maurer, J. H. M.; Kanelidis, I.; Kraus, T. Multivalent Bonds in Self-assembled Bundles of Ultrathin Gold Nanowires. *Phys. Chem. Chem. Phys.*, **2016**, *18*, 27165–27169

(27) Muratova, I. S.; Mikhelson, K. N.; Ermolenko, Yu.; Offenhäusser, A.; Mourzina, Y. On "Resistance Overpotential" Caused by a Potential Drop along the Ultrathin High Aspect Ratio Gold Nanowire Electrodes in Cyclic Voltammetry *J. Solid State Electrochem.* **2016**, *20*, 3359–3365.

(28) Kura, H.; Ogawa, T. Synthesis and Growth Mechanism of Long Ultrafine Gold Nanowires with Uniform Diameter. *J. Appl. Phys.* **2010**, *107*, 074310.

(29) Lacroix, L.-M.; Arenal, R.; Viau, G. Dynamic HAADF-STEM Observation of a Single-Atom Chain as the Transient State of Gold Ultrathin Nanowire Breakdown. *J. Am. Chem. Soc.* **2014**, *136*, 13075−13077.

(30) Takahata, R.; Yamazoe, S.; Warakulwit, C.; Limtrakul, J.; Tsukuda, T. Rayleigh Instability and Surfactant-Mediated Stabilization of Ultrathin Gold Nanorods. *J. Phys. Chem. C* **2016**, *120*, 17006–17010.

(31) Loubat, A.; Escoffier, W.; Lacroix, L.-M.; Viau, G.; Tan, R.; Carrey, J.; Warot-Fonrose, B.; Raquet, B. Cotunneling Transport in Ultra-narrow Gold Nanowire Bundles. *Nano Research* **2013**, *6*, 644–651.

(32) Imura, Y.; Hojo, S.; Morita, C.; Kawai, T. Preparation of Silica-Coated Ultrathin Gold Nanowires with High Morphological Stability. Langmuir **2014**, *30*, 1888−1892.

(33) Woehrle, G. H.; Brown, L. O.; Hutchison, J. E. Thiol-Functionalized, 1.5-nm Gold Nanoparticles through Ligand Exchange Reactions: Scope and Mechanism of Ligand Exchange. *J. Am. Chem. Soc.* **2005**, *127*, 2172-2183.

(34) Imura, Y.; Tanuma, H.; Sugimoto, H.; Ito, R.; Hojo, S.; Endo, H.; Morita, C.; Kawai, T. Water-Dispersible Ultrathin Au Nanowires Prepared Using a Lamellar Template of a Long-Chain Amidoamine Derivative. *Chem. Commun.* **2011**, *47*, 6380– 6382.

(35) Perdew, J. P.; Burke, K.; Ernzerhof, M. Generalized Gradient Approximation Made Simple. *Phys. Rev. Lett.* **1996**, *77*, 3865–3868.

(36) Blöchl, P.E. Projector Augmented-wave Method. *Phys. Rev. B* **1994**, *50*, 17953–17979.

(37) Kresse, G.; Joubert, D. From Ultrasoft Pseudopotentials to the Projector Augmented-wave Method. *Phys. Rev. B* **1999**, *59*, 1758–1775.

(38) Kresse, G.; Fürthmuller, J. Efficiency of *Ab Initio* Total-energy Calculations for Metals and Semiconductors Using a Plane-wave Basis Set. *Comput Mater Sci* **1996**, *6*, 15–50;

(39) G. Kresse and J. Fürthmuller, Efficient Iterative Schemes for *Ab Initio* Total-energy Calculations Using a Plane-wave Basis Set. *Phys Rev B* **1996**, *54*, 11169–11186.

(40) Grimme, S.; Antony, J.; Ehrlich. S.; Krieg, H. A. A Consistent and Accurate *Ab Initio* Parametrization of Density Functional Dispersion Correction (DFT-D) for the 94 Elements H-Pu. *J. Chem. Phys.* 2010, **132**, 154104;

(41) Grimme, S.; Ehrlich, S. Goerigk, L. Effect of the Damping Function in Dispersion Corrected Density Functional Theory. *J. Comput. Chem.* 2011, **32**, 1456–1465.

(42) Monkhorst, H. J.; Pack, J. D. Special Points for Brillouin-zone Integration. *Phys. Rev. B* 1976, **13**, 5188–5192.

(43) Marbella, L.E.; Millstone, J. E. NMR Techniques for Noble Metal Nanoparticles. *Chem Mater* 2015, **27**, 2721–2739;

(44) Cros-Gagneux, A.; Delpech, F.; Nayral, C.; Cornejo, A.; Coppel, Y.; Chaudret, B. Surface Chemistry of InP Quantum Dots: a Comprehensive Study. *J. Am. Chem. Soc.* 2010, **132**, 18147–18157;

(45) Ramirez, E.; Erades, L.; Philippot, K.; Lecante, P.; Chaudret, B. Shape Control of Platinum Nanoparticles. *Adv. Funct. Mater.* 2007, **17**, 2219 – 2228;

(46) Ramirez, E. ; Jansat, S. ; Philippot, K. ; Lecante, P.; Gomez, M. ; Masdeu- Bultó, A. M. ; Chaudret, B. Influence of Organic Ligands on the Stabilization of Palladium nanoparticles. *J. Organomet. Chem.* 2004, **689**, 4601 – 4610.

(47) Pearson, R. G. Absolute Electronegativity and Hardnes: Application to Inorganic Chemistry. *Inorg. Chem.* 1988, **27**, 734–740.

SUPPLEMENTARY MATERIALS

Surface-engineering of ultrathin gold nanowires: tailored self-assembly and enhanced stability

El Said A. Nouh,[†,‡] Edwin A. Baquero,[†,§] Lise-Marie Lacroix,[†] Fabien Delpech,[†] Romuald Poteau,[†] Guillaume Viau[*,†]

[†]LPCNO, Université de Toulouse, CNRS, INSA, UPS, 135 avenue de Rangueil, F-31077 Toulouse Cedex 4, France
[‡]Nuclear Materials Authority, P.O. Box 530, El Maadi, Cairo, Egypt
[§]Departamento de Química, Facultad de Ciencias, Universidad Nacional de Colombia, Sede Bogotá, Carrera 30 No. 45-03, 111321 Bogotá, Colombia

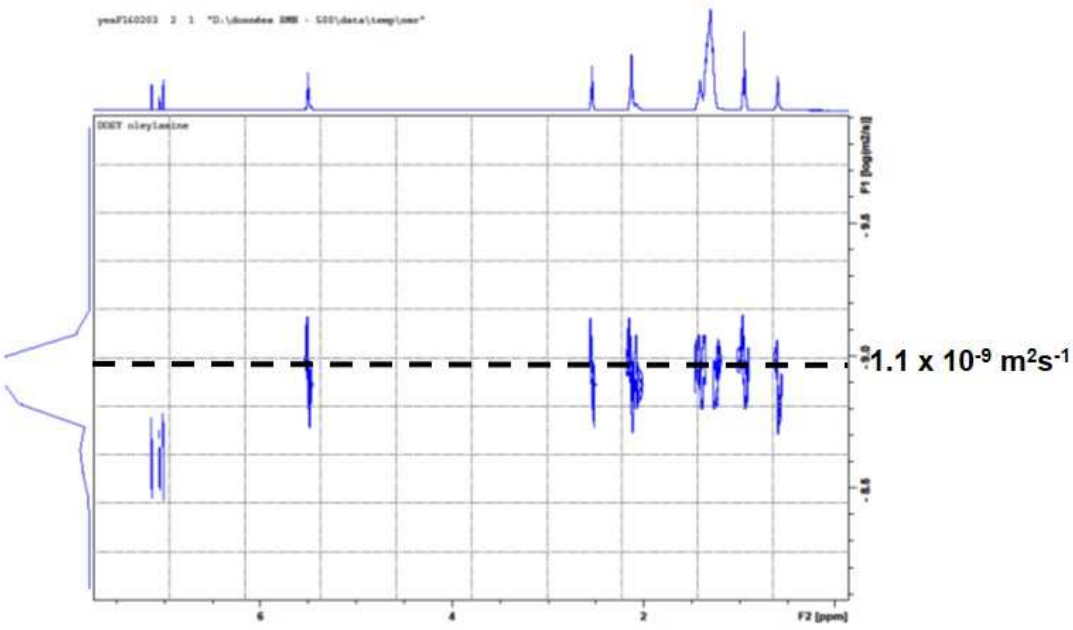

Figure S1. DOSY spectrum of pure oleylamine in toluene-d_8.

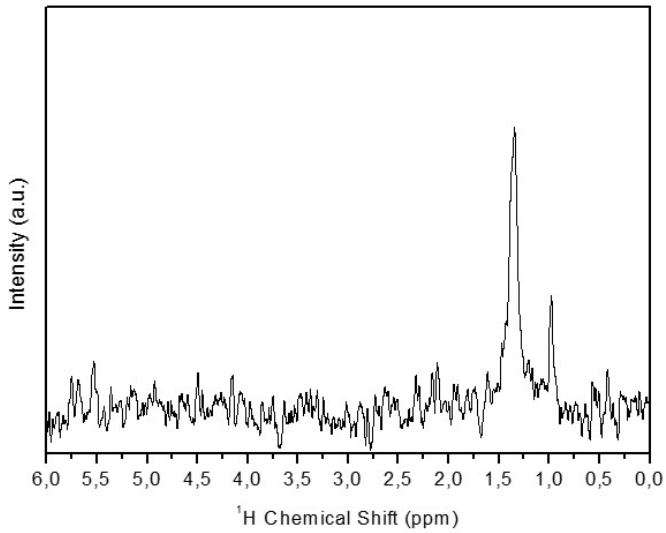

Figure S2. Diffusion filtered ^{1}H NMR spectrum of Au NWs stabilized by oleylammonium after two purifications. The spectrum corresponds to the resonance signals observed at D = 4.0 x 10^{-10} m^2s^{-1}.

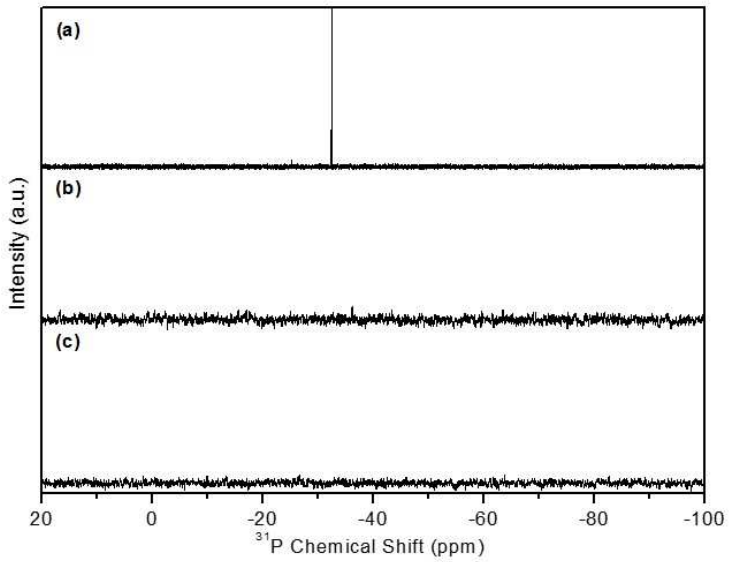

Figure S3. ^{31}P NMR spectrum of Au NWs coated with OAm: (a) after addition of TOP, (b) after one purification, and (c) after two purifications.

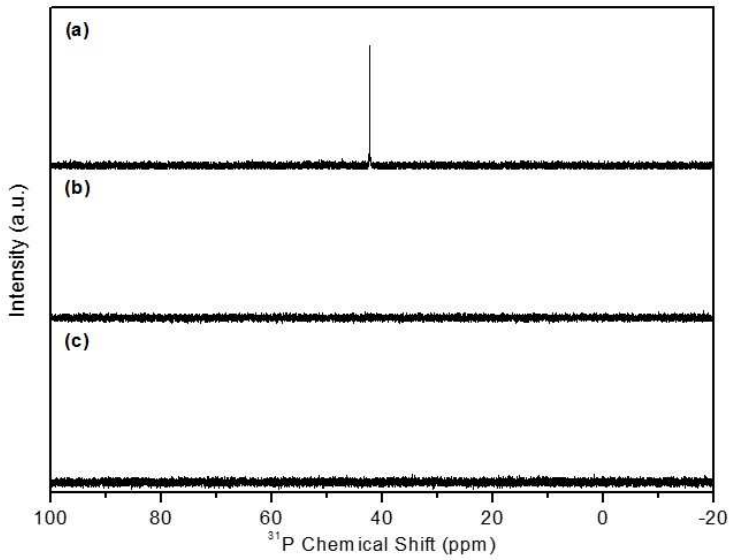

Figure S4. ^{31}P NMR spectrum of Au NWs coated with OAm: (a) after addition of TOPO, (b) after one purification, and (c) after two purifications.

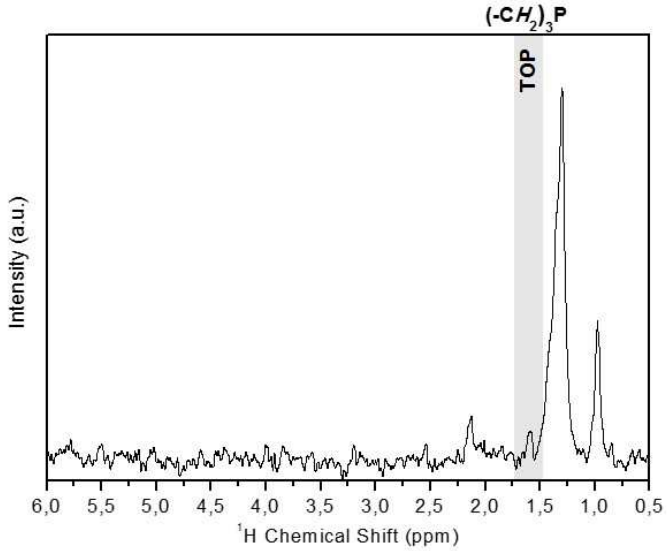

Figure S5. Diffusion filtered ^{1}H NMR spectrum of Au NWs treated with TOP after two purifications. The spectrum corresponds to the resonance signals observed at D = 2.2 x 10^{-10} m^2s^{-1}.

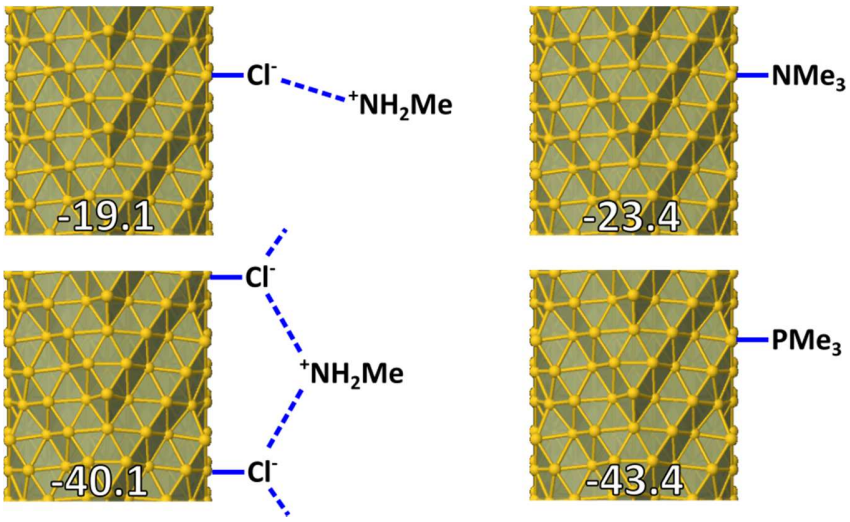

Figure S6. Adsorption energies (in kcal.mol^{-1}) and patterns of ligands on a gold nanowire.

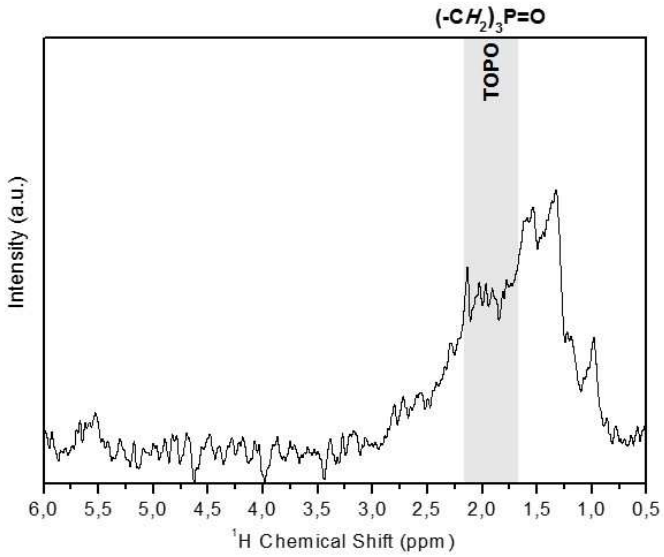

Figure S7. Diffusion filtered ^{1}H NMR spectrum of Au NWs treated with TOPO after two purifications. The spectrum corresponds to the resonance signals observed at D = 1.29 x 10^{-10} m^2s^{-1}.

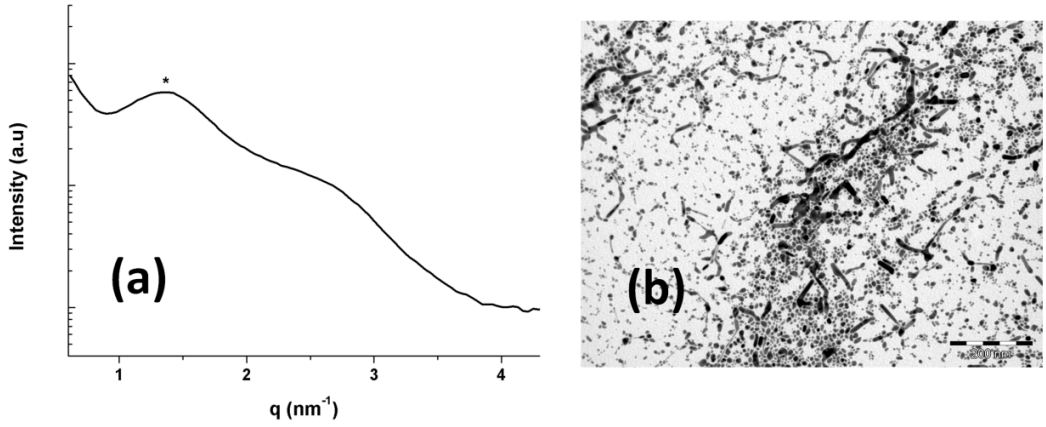

Figure S8. (a) SAXS pattern of Au NWs after ligand exchange with 1-dodecanthiol; (b) corresponding TEM image.

Theoretical part: analysis of the DFT electronic structure

This part aims at evaluating the Au-LMe_3 interaction (L=P or N) thanks to the molecular orbital language. Since the states calculated with VASP are expanded in a plane wave basis set, it is necessary to project them on a local basis set. This is achieved with the LOBSTER (Local Orbital Basis Suite Towards Electronic-Structure) package [1]. It allows calculating Crystal Orbital Hamilton Population (COHP, see Ref. 2) curves projected in a local atomic basis set (pCOHP), and also reliable atom-projected density of states (pDOS), both directly based on plane-wave wavefunctions calculated with the VASP package. Several example of the application of such analysis to ruthenium nanoclusters in equilibrium with syngas can be found in Ref. 3.

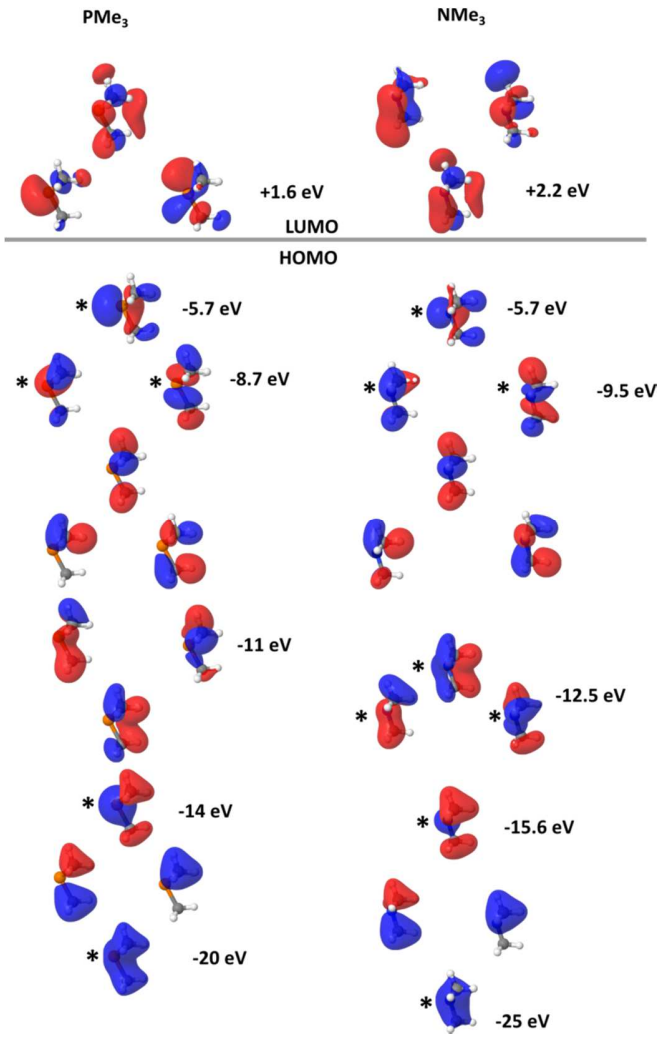

Figure S9. MOs of LMe_3 (L=P or N), calculated at the DFT-B3LYP level of theory, with the Gaussian09 package [4], within the 6-31G(d,p) basis set. The occupied MOs that are expected to be involved in the Au-LMe_3 interactions due to their significant L-axial and L-tangential character are marked with a * sign. Although the HOMO lies at the same energy in both ligands, the lone pair-like component is more diffuse on P than on N. With a slightly more stable LUMO in PMe_3 than in NMe_3, the HOMO-LUMO gap is smaller in the phosphine ligand, in line with its softer HSAB character. The other occupied MOs than can be involved in the surface-ligand interactions lie closer to the Fermi energy in PMe_3 than in NMe_3. Overall, these features are expected to involve a stronger interaction of the phosphine with the surface.

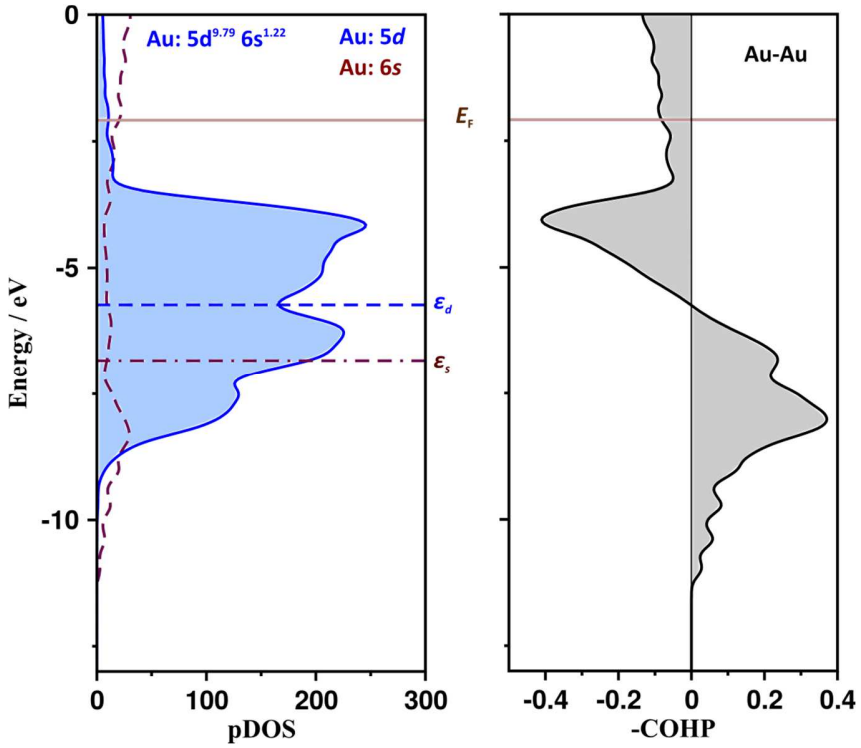

Figure S10. pDOS and pCOHP profiles for the bare AuNW (LOBSTER basis set on which the projection is done: 5*p*, 5*d*, 6*s*. Absolute charge spilling: 1.65%. This small charge spilling is not significantly reduced by adding a 6*p* subshell in the basis set). ε_d and ε_s designate the d- and s-band centers, following the seminal d-band center formulation of Hammer and Nørskov [5]. The atomic population is calculated by integration of the projected DOS. It is no surprise that it is in line with the Au(0) character of gold atoms in this bare metal nanowire.

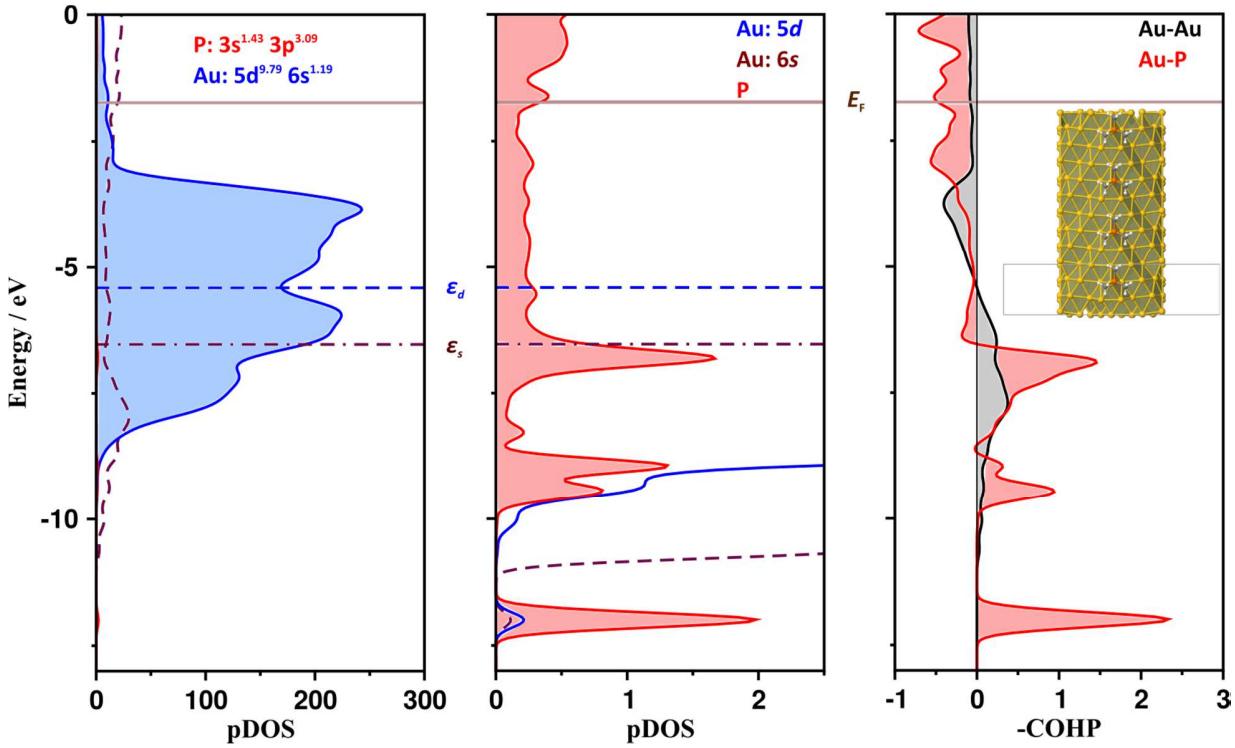

Figure S11. pDOS and pCOHP profiles for PMe_3*AuNW. The s- and d-band centers for the gold nanowire do not change much upon adsorption with respect to the bare AuNW. According to the DOS and COHP profiles, the Au-P bonding state located at *ca*. -12 eV has a strong charge transfer (CT) character, with a small component on the neighboring gold atom (blue and maroon DOS profiles), that does not exist in the naked AuNW (see DOS profile in Fig. S9). Other states higher in energy also significantly contribute to the bonding between Au and the PMe_3 ligand, whereas the states close to the fermi energy (E_F) exhibit an antibonding character. Nevertheless, the integration of COHP(ε) up to the Fermi energy indicates a net bonding interaction (ICOHP: 2.0 eV, *i.e*. 45 kcal/mol). An Au-Au interaction is much weaker, with ICOHP: 0.3 eV (7.6 kcal/mol, but mind that the coordination number of gold atoms is in the range 5 to 12). The electronic population per atom can be calculated by integrating the DOS up to the Fermi energy. The gross population on P is 4.5e, whereas the gross population on each methyl group is 7.8e, probably owing to some back-donation from the surface.

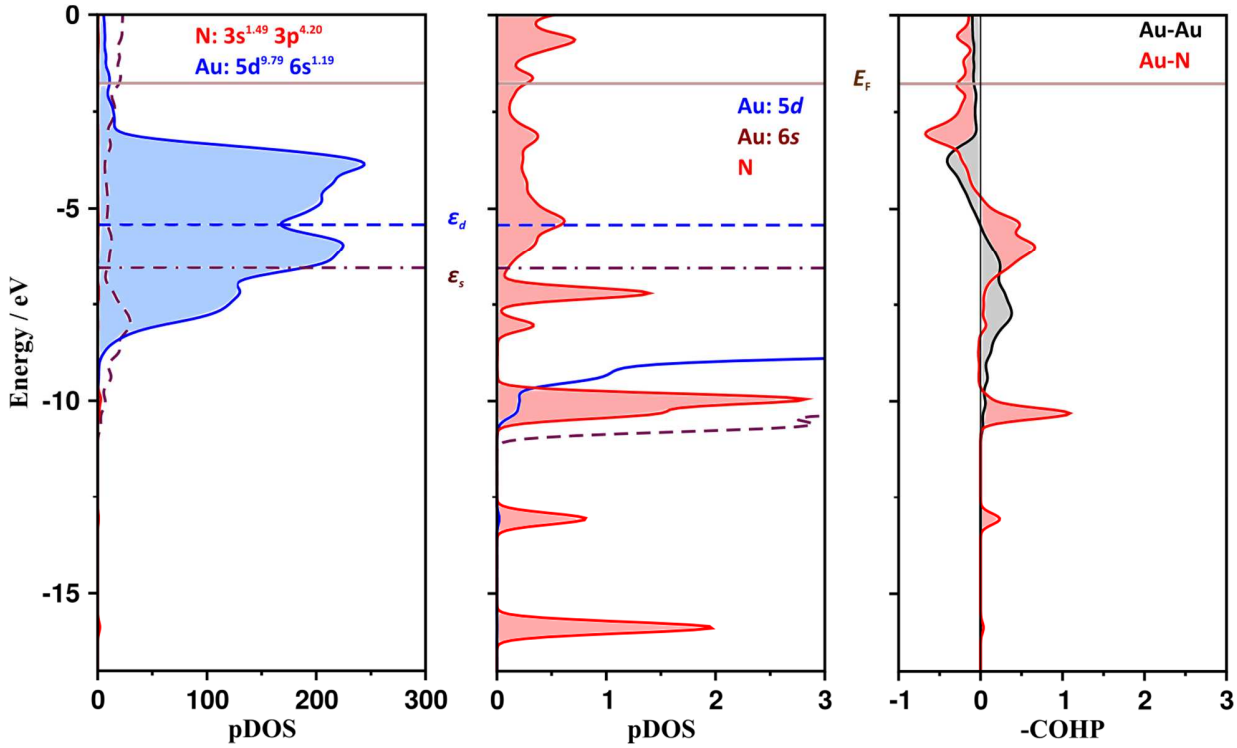

Figure S12. pDOS and pCOHP profiles for NMe_3*AuNW (COHP: same *x*-scale as in Fig. S10, for the purpose of comparison). As in PMe_3*AuNW, the s- and d-band centers for the gold nanowire do not change much upon adsorption with respect to the bare AuNW. According to the DOS and COHP profiles, there is no strong Au-N bonding state located at *ca.* -12 eV, on the contrary to what is observed in PMe_3*AuNW. According to the DOS profile, the states lying at -12.5 eV and -16 eV are localized on the ligand, with no significant contribution of the metal that could favor a LMCT state. Other states higher in energy significantly contribute to the bonding between Au and the NMe_3 ligand, whereas the states close to the fermi energy (E_F) exhibit an antibonding character. The integration of COHP(ε) up to the Fermi energy indicates a net bonding interaction weaker than PMe3 at the same site (ICOHP: 0.8 eV, *i.e.* 19 kcal/mol). The Au-Au interaction is still characterized by a weak ICOHP index: 0.3 eV (7.6 kcal/mol). The electronic population per atom can be calculated by integrating the DOS up to the Fermi energy. The gross population on N is much higher than calculated on P (5.7e *vs.* 4.5e), whereas the gross population on each methyl group is 7.5e. Overall, these results show a weaker LMCT charge transfer in the amine-protected AuNW.

References for the theoretical SI

[1] (a) Deringer, V. L.; Tchougréeff, A. L. & Dronskowski, R. Crystal Orbital Hamilton Population (COHP) Analysis As Projected from Plane-Wave Basis Sets (2011). *J. Phys. Chem. A* **115**, 5461-5466; (b) Maintz, S.; Deringer, V. L.; Tchougréeff, A. L. & Dronskowski, R. LOBSTER: A tool to extract chemical bonding from plane-wave based DFT (2016). *J. Comp. Chem.* **37**, 1030-1035.

[2] Dronskowski, R. & Blöchl, P. E. Crystal Orbital Hamilton Populations (COHP): Energy-Resolved Visualization of Chemical Bonding in Solids Based on Density-Functional Calculations (1993). *J. Phys. Chem.* **97**, 8617-8624.

[3] (a) Cusinato, L.; Martinez-Prieto, L. M.; Chaudret, B.; del Rosal, I. & Poteau, R. Theoretical characterization of the surface composition of ruthenium nanoparticles in equilibrium with syngas (2016). *Nanoscale* **8**, 10974-10992.

[4] Frisch, M. J.; Trucks, G. W.; Schlegel, H. B.; Scuseria, G. E.; Robb, M. A.; Cheeseman, J. R.; Scalmani, G.; Barone, V.; Mennucci, B.; Petersson, G. A.; Nakatsuji, H.; Caricato, M.; Li, X.; Hratchian, H. P.; Izmaylov, A. F.; Bloino, J.; Zheng, G.; Sonnenberg, J. L.; Hada, M.; Ehara, M.; Toyota, K.; Fukuda, R.; Hasegawa, J.; Ishida, M.; Nakajima, T.; Honda, Y.; Kitao, O.; Nakai, H.; Vreven, T.; Montgomery Jr., J. A.; Peralta, J. E.; Ogliaro, F.; Bearpark, M.; Heyd, J. J.; Brothers, E.; Kudin, K. N.; Staroverov, V. N.; Kobayashi, R.; Normand, J.; Raghavachari, K.; Rendell, A.; Burant, J. C.; Iyengar, S. S.; Tomasi, J.; Cossi, M.; Rega, N.; Millam, J. M.; Klene, M.; Knox, J. E.; Cross, J. B.; Bakken, V.; Adamo, C.; Jaramillo, J.; Gomperts, R.; Stratmann, R. E.; Yazyev, O.; Austin, A. J.; Cammi, R.; Pomelli, C.; Ochterski, J. W.; Martin, R. L.; Morokuma, K.; Zakrzewski, V. G.; Voth, G. A.; Salvador, P.; Dannenberg, J. J.; Dapprich, S.; Daniels, A. D.; Farkas., Ö.; Foresman, J. B.; Ortiz, J. V.; Cioslowski, J. & Fox, D. J. Gaussian 09 Revision D.0.

[5] Hammer, B. & Nørskov, J. K. Electronic Factors Determining the Reactivity of Metal Surfaces (1995). *Surf. Sci.* **343**, 211-220.